

Optical and Electrical Properties of Cu-ZnO Prism Shaped Nanocrystals by Microwave Combustion Method

Vidyasagar C. C^{1,*}, Gururaj Hosamani², Prakash Kariyajjanavar³

¹Department of Chemistry, Rani Channamma University, Belgaum-591 156, India

²Department of Electronics, Kuvempu University, Shankaraghatta-577 451, India

³Department of Environmental Science, Gulbarga University, Kalaburagi-585106, India

*Corresponding author: vidya.891@gmail.com

Received September 04, 2019; Revised October 14, 2019; Accepted October 28, 2019

Abstract Dye-sensitized solar cells (DSSCs) are a low cost and promising alternative to standard silicon photovoltaic cells; there is growing interest in near-infrared sensitization of semiconductor anode materials, which converts to high power conversion efficiencies (PCEs). In this work, the effect of ion implantation and annealing temperature has been studied to provide an effective approach for developing visible-light driven Cu-ZnO anode materials for solar cells. Synthesis of ZnO and Cu doped ZnO nanoparticles via microwave combustion method without using any fuel is proposed. The crystal structure, optical properties, surface morphology and electrical properties were characterized by X-ray diffraction (XRD), UV-Vis spectroscopy, scanning electron microscopy (SEM), energy dispersive X-ray spectroscopy (EDAX) and Keithley Source meter. The results revealed that the change in lattice parameters, decrease in the band gap and absorption peak shifting towards near-infrared region are due to the change in concentration and annealing temperature. The change in crystal defects leads to an abrupt change in bond length, unit volume and lattice strain in the Cu-ZnO crystals. Optical absorbance of copper phthalocyanine pigment (Imperon Blue-15) sensitized Cu-ZnO films were found to be at 600 nm to 700 nm region.

Keywords: crystal structure, doping, Imperon Blue, I-V characteristics, zinc oxide

Cite This Article: Vidyasagar C. C, Gururaj Hosamani, and Prakash Kariyajjanavar, "Optical and Electrical Properties of Cu-ZnO Prism Shaped Nanocrystals by Microwave Combustion Method." *American Journal of Energy Research*, vol. 7, no. 1 (2019): 31-40. doi: 10.12691/ajer-7-1-4.

1. Introduction

Nowadays, the dye-sensitized solar cells (DSSCs) have been considered as an alternative for the conventional solar cells in various aspects such as low-cost fabrication process. It is crucial to improve the cost-effective process and utilization of longer wavelength is of significance for exploiting efficient hybrid materials. Among all the metal oxide semiconductors, ZnO will be considered as the most significant and compatible multifunctional materials for dye sensitized solar cells [1], fuel cells [2], batteries [3], bio-sensors, photodiodes and photocatalysis [1,2,3]. To extend its optical absorbance band into the longer wavelength range, doping of metal ions has been carried out to create ZnO photoactive layer under UV-Vis light irradiation [4,5]. Doping of transition metal ions is a powerful tool to tailor the optical and electrical properties of semiconductors [6,7]. Selective doping of such elements as Cu, Cr, Co, Ni, Mn, Cd and Fe offers various transitions, which modify the lattice structure and optical properties of ZnO crystals. Among all dopants, copper is the most efficient doping element to modify the structure and optical properties of ZnO crystals. Recently, the results obtained for band gap tailored ZnO

crystal have shown a drastic change in the optical, magnetic and electrical properties upon doping of Cr [8], Fe [9], Co [10] and Cu [11]. Copper ion doping into the ZnO lattice modifies the photoluminescent and electrical properties by creating copper energy levels in the crystal [12,13]. In addition, Cu behaves as n-type in ZnO lattices, which makes it good p-type ZnO material [14,15]. Therefore, it is required to reduce the band gap of ZnO towards longer wave length region. Recent studies have explained the charge transfer phenomenon from ZnO energy states to Cu Fermi level [16]. Many researchers have reported *n* number of methods to optimize the existing expensive experimental protocol for the preparation of oxides of desired shapes [16,17] such as sol-gel [18], microwave [19], solid state techniques [19], hydrothermal [20] and spray pyrolysis [21], template-assisted growth [21]. Among all conventional methods, the microwave synthesis reduces the chemical reaction steps by several orders of magnitude and restrains side reactions [22]. The microwave solid-state reaction (SSR) method controls the morphology and dimension without using expensive solvents, fuels and multifaceted instruments [23]. In SSR molecular dipoles react with microwave radiations continuously to acquiescence themselves. In addition, surfactant (ethylene glycol) in SSR decides the morphology. This dipole spinning relative to the frequency of the

irradiation loses its energy through molecular dielectric friction [22]. Several groups have been used near IR dyes as sensitizers in DSSCs obtaining rather low conversion efficiencies. This is mainly due to the formation of aggregates and difficulties to obtain dyes with appropriate energy levels of the excited states. A number of dyes and pigments have been synthesized to improve the absorption edge towards IR region, which could generate the number of effective electrons [24].

Therefore, this work is aimed at low-cost technology for the preparation of Cu-ZnO crystal and to study the effect of Cu^{2+} on the structural and optical properties of pyramid shaped ZnO crystal at different annealing temperature. Wang et al. reported that, Cu^+ ion could be a reason for increasing crystal size. In our case Cu^{2+} ion is more preferable to replace the Zn^{2+} ions in ZnO lattice, which enhances the maximum absorption peak towards the NIR region.

2. Experimental

Zinc nitrate hexahydrate [$\text{Zn}(\text{NO}_3)_2 \cdot 6\text{H}_2\text{O}$] was procured from Himedia Laboratories Pvt. Ltd., and ethylene glycol was procured from Sd-Fine-Chem Ltd. (Mumbai, India). All the chemicals were of analytical grade and were used as received without further purification. Double distilled water was used for the preparation of solutions. The synthesis of pyramid shaped ZnO structures was carried out in a domestic microwave oven (Onida Power Solo 17D) operating at 40 % power of 800 W. Copper phthalocyanine [CAS No. 147-14-8] ($\text{C}_{32}\text{H}_{16}\text{CuN}_8$) was sensitized on Cu-ZnO films, which was procured from Dye Star Company, Mumbai.

2.1. Synthesis of Pyramid-shaped ZnO Nanostructures

In a typical synthesis, 30 g of zinc nitrate hexahydrate was mixed in a dry beaker containing minimum amount (2 mL) of ethylene glycol. Initially the mixture was stirred vigorously using a glass rod and placed in a domestic microwave oven. The solution was exposed to the microwave energy 2300 MHz and 40% power for 6 min. Initially, the reaction mixture was boiled and subsequently it underwent dehydration followed by decomposition with the evolution of heat and gases (O_2 , NO_2) with pale orange color fumes. The combustion was completed within 10 min resulting in the formation of a white porous powder of ZnO. The resulting solid was subsequently annealed at 450 °C in a muffle furnace and finally a fine crystalline powder of ZnO was obtained. Similar procedure has been followed for the synthesis of Cu doped ZnO nanoparticles at different temperature.

2.2. Fabrication of P-type Anode Electrodes

As synthesized metal oxide semiconducting nanoparticles were used to prepare films by doctor blade method. Glass plate of 2 cm × 2 cm dimension was used as a substrate. Metal oxide semiconducting nanoparticles (500 mg) were dispersed in 1:1 water and ethanol (v/v) system by sonication followed by stirring until gelatine occurred

(5 min) to obtain a paste of appropriate viscosity. The resultant paste was coated on a transparent glass plate by doctor blade method using a scotch tape as a spacer. The paste was flattened uniformly with a thin blade and then annealed at 80°C for 30 min in air to eliminate water and alcohol adsorbed on the semiconductor surface. Dye solutions of 0.5 mM were prepared using dilute ethanol and water system (20 mL alcohol + 5 mL water) (Figure 1). Semiconductor films were immersed into dye solution for 1 h to coad the dye on the surface of semiconductor electrodes. After dye adsorption, the films were exposed to sunlight for 30 min. Then UV-Vis absorbance was recorded for all the samples to investigate the light response.



Figure 1. Shows the fabrication of dye sensitized sample by doctor-blade method

2.3. Characterization of Nanostructures

XRD patterns were recorded on a Philips X'Pert X-ray diffractometer using $\text{CuK}\alpha$ radiation. The size distribution, structural and surface morphology of the samples were analyzed by field emission scanning electron microscope (FE-SEM) equipped with an energy dispersive X-ray spectroscopy (EDAX), model: Nova Nano SEM600-FEI. The optical absorbance and photoresponse of pure and doped samples was measured on a UV-Vis spectrophotometer, model: USB 4000, Ocean Optics, USA. I-V characteristics were studied by Keithley source meter with USB GRIB adaptor, model: 2401.

3. Results and Discussion

3.1. Structural Analysis

The change in the structural morphology has been reflected by the variations in XRD patterns of as-synthesized samples (Figure 2A and Figure 2B). All the diffraction peaks in the XRD correspond to JCPDS Card No. 80-0075 of hexagonal wurtzite having lattice parameters $a = 3.2500 \text{ \AA}$ and $c = 5.2079 \text{ \AA}$ (Figure 1a). No contamination (CuO or Cu_2O) peaks have been observed in any of the Cu doped ZnO samples within the detection limit (Figure 2b to Figure 2d). The slight variation in the lattice parameter of the same phase can be attributed to the change in the crystallite size in the doped samples. The peak positions are shifted slightly to the right (higher angle) (Figure 2b) as compared to pure ZnO (Figure 2a) [1]. This shift in the peaks position illustrates the incorporation of Cu into the lattice of ZnO. The full width at half maximum peaks (1 0 0) and (2 0 0) are found to be decrease with increasing intensity for the doped samples and continuous to decrease with increasing dopant concentration. This results, there is a observable

change in lattice parameter c , but apparent increase in lattice parameter a , which indicates clearly that the Cu doping distorted both a and c parameters in ZnO lattice, which in turn caused the reduction of unit cell volume [1]. It is attributed to the substitution of Zn^{2+} ions by Cu^{2+} ions. At higher concentration of Cu^{2+} , even though it replaces Zn^{2+} ions but also it may enter into the interstitial planes of ZnO, which causes sudden increase in the unit cell volume and dimension with Zn-O-Cu bonding structure [25] (Figure 2b). This evidently shows the irregularity in the crystallite structure. The lattice constants a and c were found to be 3.2509 Å and 5.2073 Å, respectively. As for Cu-ZnO, the lattice constant a decreased to 3.2491 Å and c decreased to 5.2038 Å. The d-spacing of the lattice fringes of the ZnO pyramid structures is 2.8154 Å for (1 0 0) and 2.6036 for (0 0 2) planes. For Cu doped ZnO d-spacing found to be decreased to 2.8138 and 2.6019 Å, respectively (Figure 2b). The shrinkage of lattice cell and d spacing after doping is due to the substitution of Zn^{2+} by smaller Cu^{2+} in (1 0 0) and (2 0 0) planes [1]. The Cu can exist in Cu^+ , Cu^{2+} and Cu^{3+} ions having ionic radii 0.077 nm, 0.073 nm and 0.054 nm, respectively. The data show that the lattice parameters a and c decreases gradually up to 1.6 % (Figure 4) due to the substitution of Cu^{2+} ions into the Zn^{2+} ions sites. Since the ionic radius of Cu^{2+} (0.73 Å) is slightly smaller than of Zn^{2+} (0.74 Å), hence, the Cu^{2+} ions are incorporated uniformly into the lattice in substitution mode, but not in interstitial mode. The slow increment in the lattice parameter “ a and c ” for concentration of 2.5 % to 5 % (Figure 2Bd and Figure 3Be) reveals the substitution of more Cu^{2+} (0.073 nm) due to smaller ionic radius compare to Cu^+ ion (0.77 nm) in Zn^{2+} (0.74 nm). From the results, we observe both Cu^+ and Cu^{2+} ions incorporated into ZnO crystal at 2.5 % of Cu concentration. When Cu is entered into the lattice, Cu^{2+} placed into the position of Zn^{2+} , which leads to a reduction in the lattice constants. However, the incorporation of copper does not influence the structure of hexagonal pyramid shaped ZnO. But, the defects were found while crystal growth. The crystal defected points are chemically active sites, where crystal starts growing through the nucleation of particles. Usually, ZnO grows preferentially along [1 0 0] direction in aqueous solution because of the lowest surface energy of (1 0 0) facet. The ionic surfactant reduces the surface energy of the polar surfaces, which resulted in the growth mechanism of the hexagonal micro pyramid along (1 0 0) axis [26]. It means that the growth mechanism starts from the same point on the base surface. However, comprehensive crystal growth process is very difficult to examine. In many cases, time dependent experiments results do not reflect accurately on intermediate crystals, because it is very difficult to immediately stop the crystal growth during the reaction [27]. The intensity of (1 0 0) and (0 0 2) peaks gradually increases with increase in annealing temperature (Figure 3Be to Figure 3Bg). However, the peak intensity of the sample annealed at 600 °C was found to be increased (Figure 3Bf). Figure 3A and Figure 3B illustrate the changes in (1 0 0) and (0 0 2) peaks position. As shown in Figure 3Be to Figure 3Bg), when the calcinations temperature increased from 450°C to 600 °C, the peaks slightly shifted towards lower angles

(Figure 3Bf). On the other hand the strongest shift towards higher angles has been observed in the sample annealed at 750 °C (Figure 3Bg). These shifts are associated directly with the changes in the lattice and gradual enhancement of crystal growth along both a and c -axis (Figure 4).

3.2. Surface Morphology Analysis

The surface morphology of all ZnO and Cu-ZnO have been studied by FE-SEM, as shown in Figure 5, Figure 6 and Figure 7. During the crystal growth, the polar surfaces usually appear as growing surface areas, because of their high surface energy. By controlling the doping level (Figure 5a to Figure 5d), it is possible to alter the growth path of ZnO structures; the highest growth rate is usually along c -axis (0 0 1) and the growth rate along [1 0 0] directions is slower than that in [0 0 2] direction, resulting in pyramid morphology (Figure 7e). In case of dopants, copper serves as structure-directing agent to adsorb selectively on ZnO basal planes and modify the surface morphology and crystal growth. For example, Cu^{2+} ions adsorbed on the (1 0 0) facets of ZnO crystals (Figure 7e and Figure 7f) would significantly decreases the growth rate of these facets. The strong interaction between the ions of the ionic liquids (ethylene glycol) and the polar surfaces form O^{2-} and Zn^{2+} ions stock up layer by layer alternatively along the c -axis. The oppositely charged ions produce positively charged zinc and negatively charged oxygen surfaces, resulting in dielectric, dipole moment and spontaneous polarization along the c -axis as well as a difference in the surface energy. Interestingly these polar surfaces make up hexagonal pyramid as shown in Figure 6. The hexagonal pyramid has O-terminated surfaces for the base and O-terminated planes of the side surfaces, which are all polar surfaces. The Zn polarized direction is along the tip of the hexagonal pyramid structure. Due to the strong electrostatic interaction between the ions of the ionic surfactants (ethylene glycol) and the polar surfaces, the surface energy of the basal polar planes may decrease greatly in comparison to those of other crystal faces, resulting in a slow growth rate for those polar planes. Therefore, the base of the ZnO hexagonal micropillar is the (0 0 2) plane [29]. The rate of particle aggregation is a key factor that controls the surface morphology and structure of the ultimate product. As the annealing temperature increased, the Cu^{2+} ions might get bonded on the surface through nucleation process. The crystal growth of Cu-ZnO pyramids along c -axis depends upon the surface polarity of Zn^{2+} and O^{2-} . This polarity arises due to the chemical potential difference between Zn^{2+} and O^{2-} at terminated surfaces. Substitution of electropositive Cu^{2+} ion in place of Zn^{2+} ions in the ZnO lattice would increase the polarity of O^{2-} along the c -axis since Cu^{2+} ions get attracted O^{2-} to a greater extent than the Zn^{2+} ions. This shows that the growth of crystals along the c -axis is more feasible. Under these conditions the controlling step of the reaction will convert to grain growth to crystal nuclei formation, which leads to an increase in nuclear aggregation caused by the rapid formation of aggregates among the crystal nuclei (Figure 7g and Figure 7h). Figure 8 shows the energy dispersive X-ray patterns of ZnO, which show the presence of pure zinc and oxygen in ZnO nanostructures.

The EDAX spectra of Cu-ZnO (Figure 8b and Figure 8d) show evidence for the presence of copper, zinc and oxygen. A small carbon peak was appeared due to carbon

tape pasted on copper grids used for the surface morphology and elemental analysis (Figure 8b to Figure 8d).

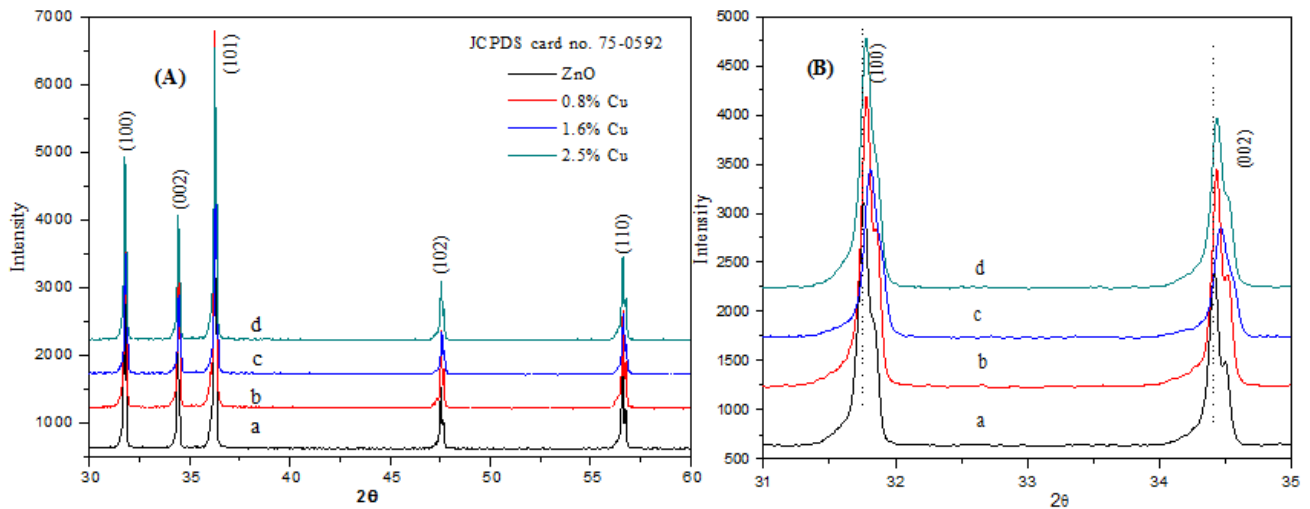


Figure 2. (A) Powder XRD pattern of ZnO and Cu-ZnO prepared at different wt% of copper, (B) Inset view of powder X-ray diffraction pattern of (1 0 0) and (0 0 2) planes

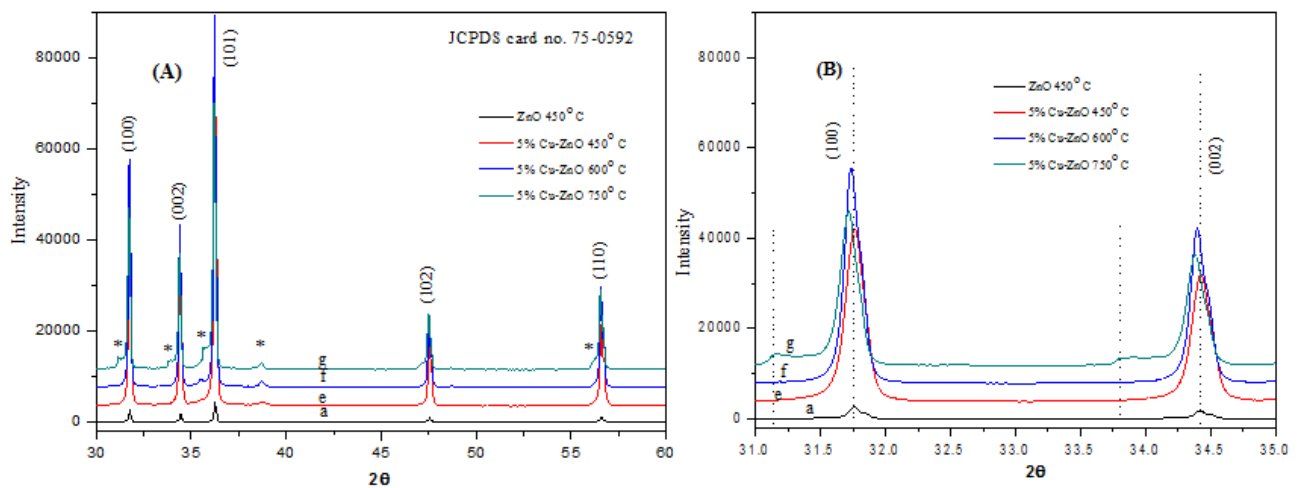


Figure 3. (A) Powder X-ray diffraction pattern of ZnO and Cu-ZnO prepared at different annealing temperature, (B) Inset view of powder X-ray diffraction pattern of (1 0 0) and (0 0 2) planes

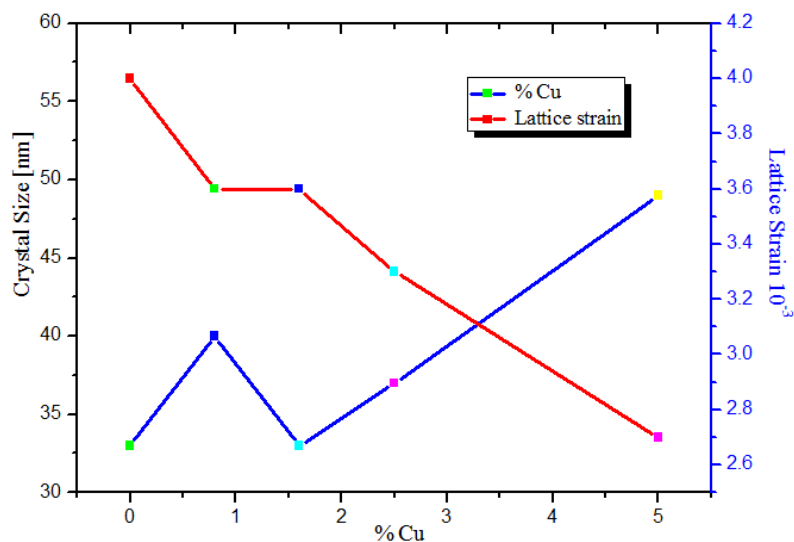


Figure 4. Lattice strain and crystallite size of ZnO and $Cu_{1-x}Zn_xO$ at different concentration

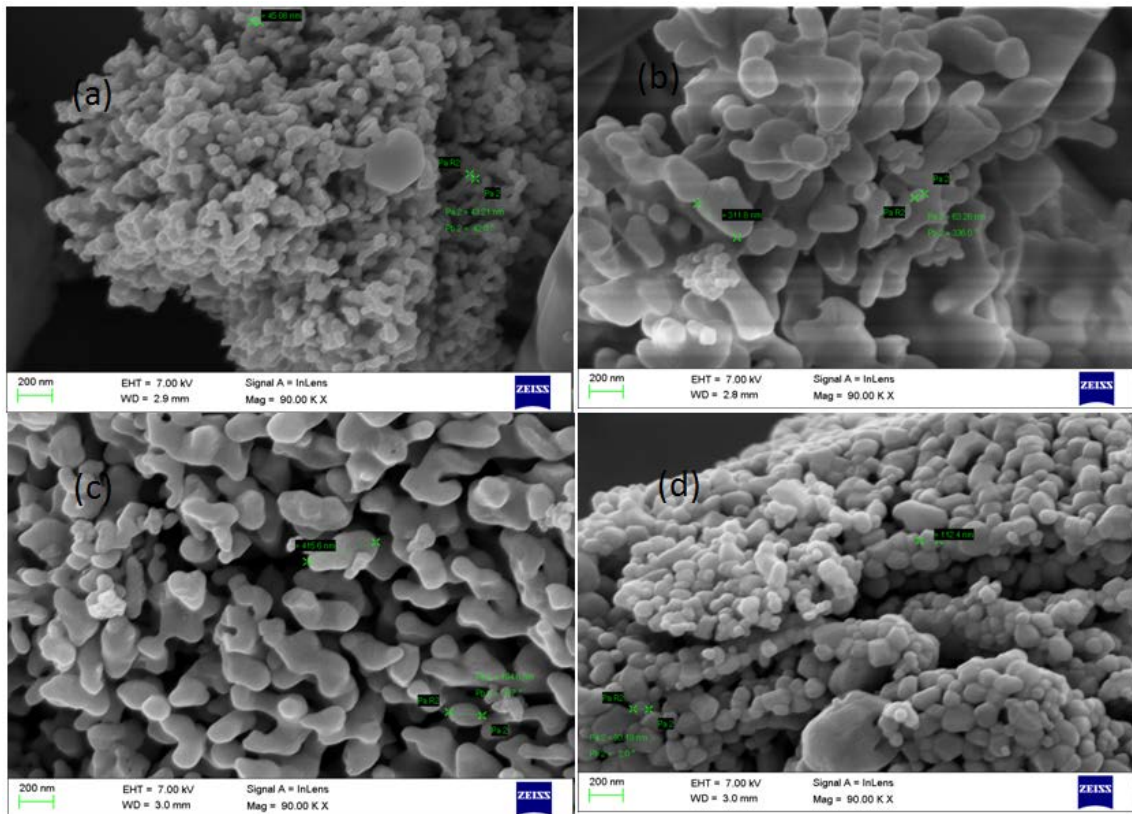


Figure 5. FESEM images of as prepared ZnO and $Cu_{1-x}Zn_xO$ at different concentration

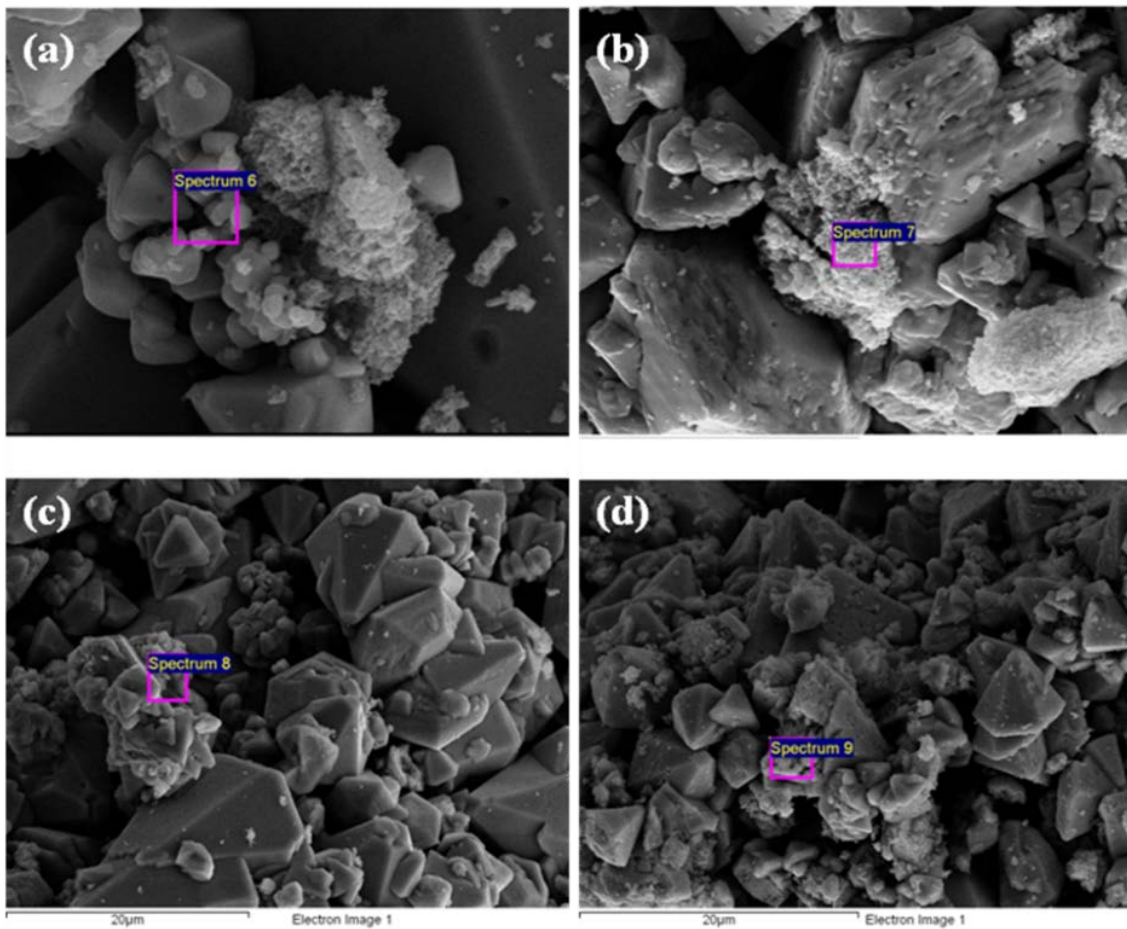


Figure 6. FESEM images of hexagonal pyramid samples prepared ZnO and $Cu_{1-x}Zn_xO$ at different concentration at lower resolution (20 μm) of Figure 7

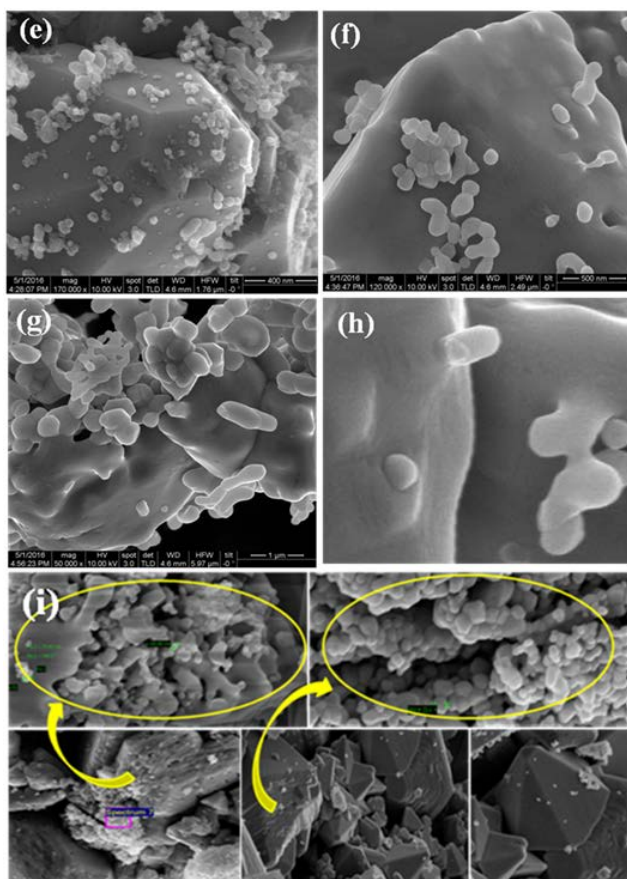


Figure 7. FESEM images of hexagonal pyramid samples prepared ZnO and $\text{Cu}_{1-x}\text{Zn}_x\text{O}$ at different annealing temperature

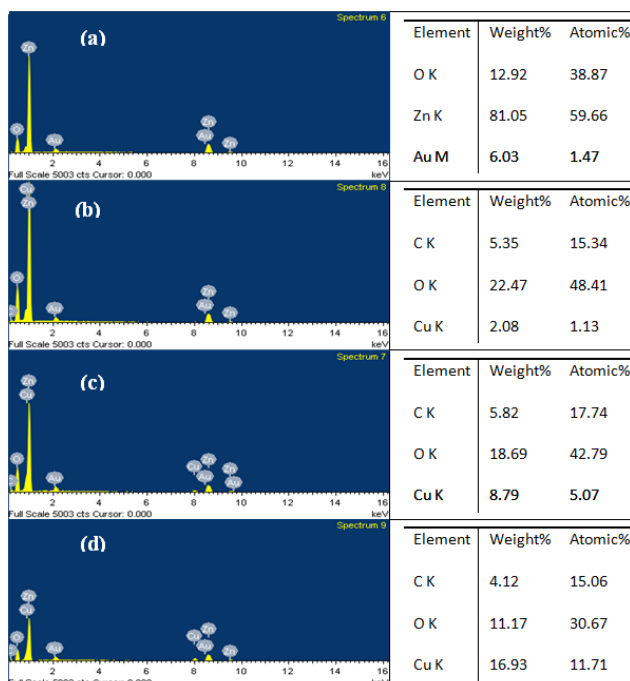


Figure 8. EDAX spectra of hexagonal pyramid samples prepared ZnO and $\text{Cu}_{1-x}\text{Zn}_x\text{O}$ at different concentration

3.3. Optical Properties of Dye Sensitized Films

Figure 9 exhibits the UV-Vis absorption spectra of pure ZnO and Cu ion doped ZnO crystals. The optical

absorption of pure ZnO was recorded in the ultraviolet region (375 nm). The all Cu-ZnO samples were found to be in the longer wavelength region, which reveals gradual red shift as the concentration increased (Figure 9). Lan Chen et al. [29] noticed that the absorbance depends upon some factors, such as particle size, oxygen deficiency, defects in grain structure, lattice strain, thickness etc. The shift in the absorption peak describes the decrease in the band gap is due to the secondary electronic states which are formed by doping of Cu ions and from transition between partially forbidden valence band and conduction band (Table 1). Figure 10 shows the UV-Vis absorption spectra of the samples annealed at different temperatures. The Cu-ZnO samples annealed at higher temperature exhibits significantly lower absorption edge, which is shifted towards the longer wavelength region (IR range) compared to the samples annealed at lower temperature [1]. As the annealing temperature increased from 450 °C to 750°C, the absorption edge shifted towards longer wavelength region, because of increase in the crystallite size at higher sintering temperature [30] (Figure 10). The optical band gap (E_g) of the Cu-ZnO was determined by using the formula, $E_g = hc/\lambda$, where h is Planck constant, c is velocity of light and λ is wavelength [1,31], where the conduction type of Cu-ZnO lattice depends on annealing temperature (Figure 10). Moreover, the reduction in the band gaps were recorded from 2.16 eV to 1.84 eV (Table 1) as the crystallinity gradually increased. The observed results show that the annealing temperature is extremely important in understanding the band gap arrangement. The optical properties of the Imperon Blue-15 (IB) dye sensitized Cu-ZnO films were also investigated by UV-Vis spectroscopy for the same samples. The absorption spectra of the adsorbed Imperon Blue-15 (IB) dye present on the surface of Cu-ZnO exhibit obvious red shift compared to the pure Cu-ZnO films. Figure 12 shows that, the absorption peak of photoanode is broader than that of the pure dye (IB-15). The shift in absorption edge near IR after dye sensitization (800 nm) is due the change in the energy of the lowest unoccupied molecular orbital (LUMO), causing $\pi \rightarrow \pi^*$ and $d\pi \rightarrow \pi^*$ transitions to occur at higher or lower energies [32] (Figure 13). Injection of additional electrons from the dye to the Cu-ZnO due to the presence of conduction band edge of Cu-ZnO is just below the LUMO state of the copper phthalocyanine pigment [33]. The transfer of electrons from the ground state of the dye located in the semiconductor energy gap into the excited state occurs, which is in resonance with the conduction band of Cu-ZnO (inset of Figure 13). In addition to that, the direct injection of electrons from the excited LUMO state of copper phthalocyanine pigment into the semiconductor CB state takes place, because of the strong bonding of the copper phthalocyanine pigment on the semiconductors surface (Figure 13).

3.4. Electrical Properties

The measured dark and UV-Vis illuminated I-V characteristics of ZnO and Cu-ZnO crystals are shown in Figure 14. Ohmic behavior and non-linear behavior of the I-V curves of ZnO and Cu-ZnO particles were observed in the dark and under UV-Vis illumination, respectively. The presence of impurities and asymmetry in the lattice may

alter the effective potential barrier and inhibit the stream of charge carriers at the grain boundaries [33]. These boundaries act as active sites and potential walls which lead to reduction of the carrier mobility by increasing resistance and decreasing the conductivity (Figure 14Bd). The abrupt fluctuation and increase in electron concentration at different concentrations of impurities is due to the Burstein-Moss effect (Figure 14Bd and Figure 14Cd). On the other hand, the reduction of photocurrent is due to the diffusion of depletion (junction) layer, when the concentration of minority carriers at the interface exceeds the majority carrier concentration at the grain boundaries, the recombination at the interface leads to loss of photocurrent (Table 1). Thus, the modification of surface morphology, increase in the crystallinity and decrease in the recombination rate can become the dominant mechanism accounting for enhancing photo-current (Figure 14Cf and Figure 14Cg). Under UV-illumination minority carrier build up at the semiconductor interface due to slow charge transfer [28] (Figure 14A and Figure 14C). The current at a voltage of 4 V for the films under UV-illumination is higher than that under dark conditions. The forward current increases nonlinearly with forward bias voltage (Figure 14B and Figure 14D). This indicates that the UV-Vis illumination increases the production of electron-hole pairs at room temperature ($T \sim 30\text{ }^{\circ}\text{C}$). The resistivity was decreased by doping of Cu into ZnO lattice (0.8 wt.% to 5.0 wt.%) under UV-Vis illumination (Figure 14D). Moreover, at a certain doping concentration of Cu the neutral defects may be observed. These defects neutralize the excess charge carriers (Figure 14Bd) under UV-Vis illumination, which may enhance the resistivity [34]. Additionally, the reverse saturation current (I) increases with the increasing doping percentage of Cu at 0.8 % and 1.6 % (Figure 14Bd and Figure 14Cg) and decreases at 2.5 % in the Cu-ZnO film. Under suitable conditions (Figure 14D), the UV-Vis light illuminating the prepared films of Cu-ZnO increases the conductivity due to increase the mobility of charge carriers at higher temperature due to increase in crystallinity (Table 1). As the crystallinity increases at higher temperature, significantly it improves the conductivity and decreases the resistivity of the Cu-ZnO films. This shows the significant characteristic relationship between the resistance and conductance of the pure ZnO and Cu doped ZnO nanoparticles.

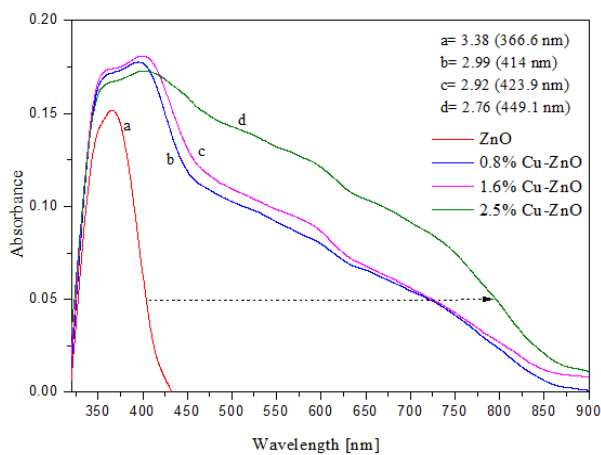


Figure 9. UV-Vis absorption spectra of hexagonal pyramid samples prepared ZnO and $\text{Cu}_{1-x}\text{Zn}_x\text{O}$ at different concentration

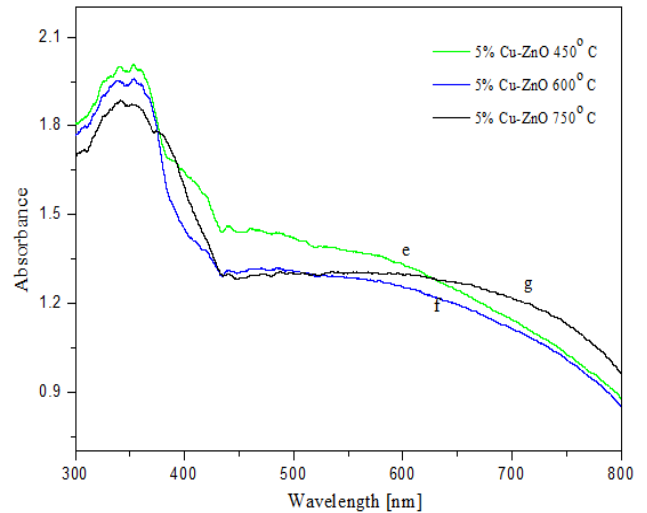


Figure 10. UV-Vis absorption spectra of hexagonal pyramid samples prepared ZnO and $\text{Cu}_{1-x}\text{Zn}_x\text{O}$ at different annealing temperature

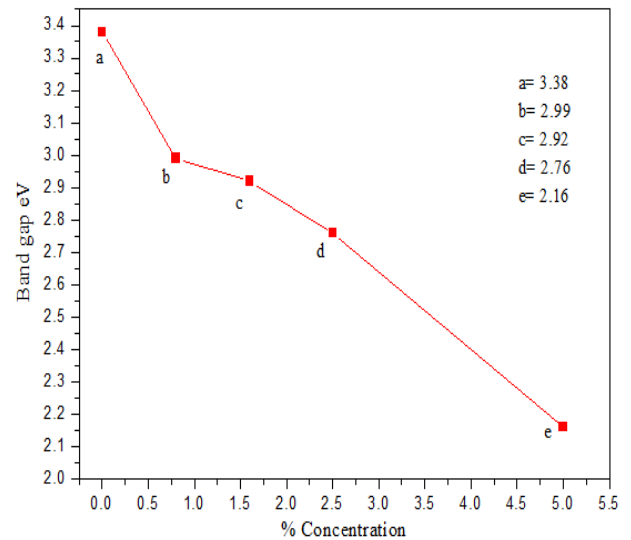


Figure 11. Band gap of as-prepared ZnO and $\text{Cu}_{1-x}\text{Zn}_x\text{O}$ nanocrystals at different concentration

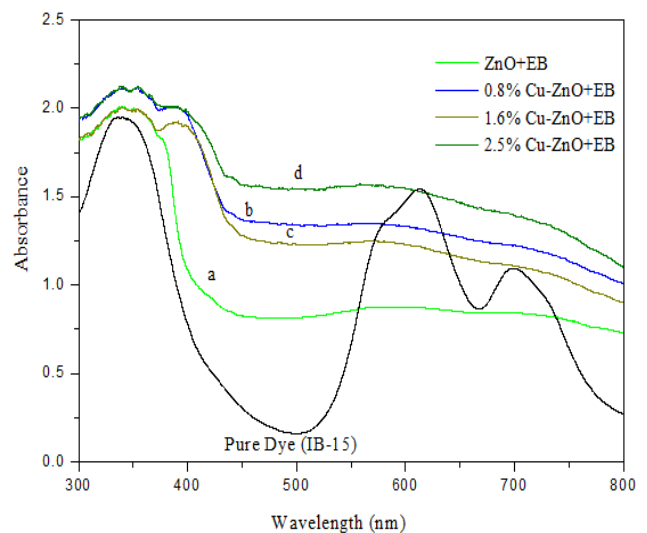
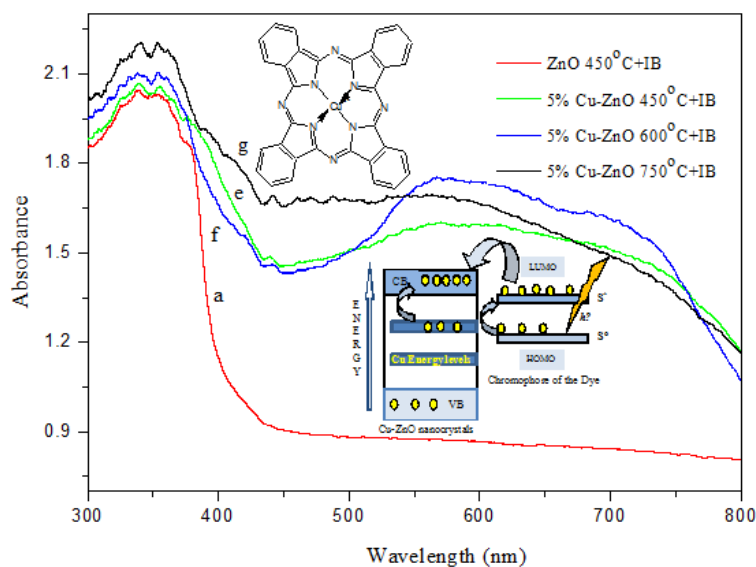
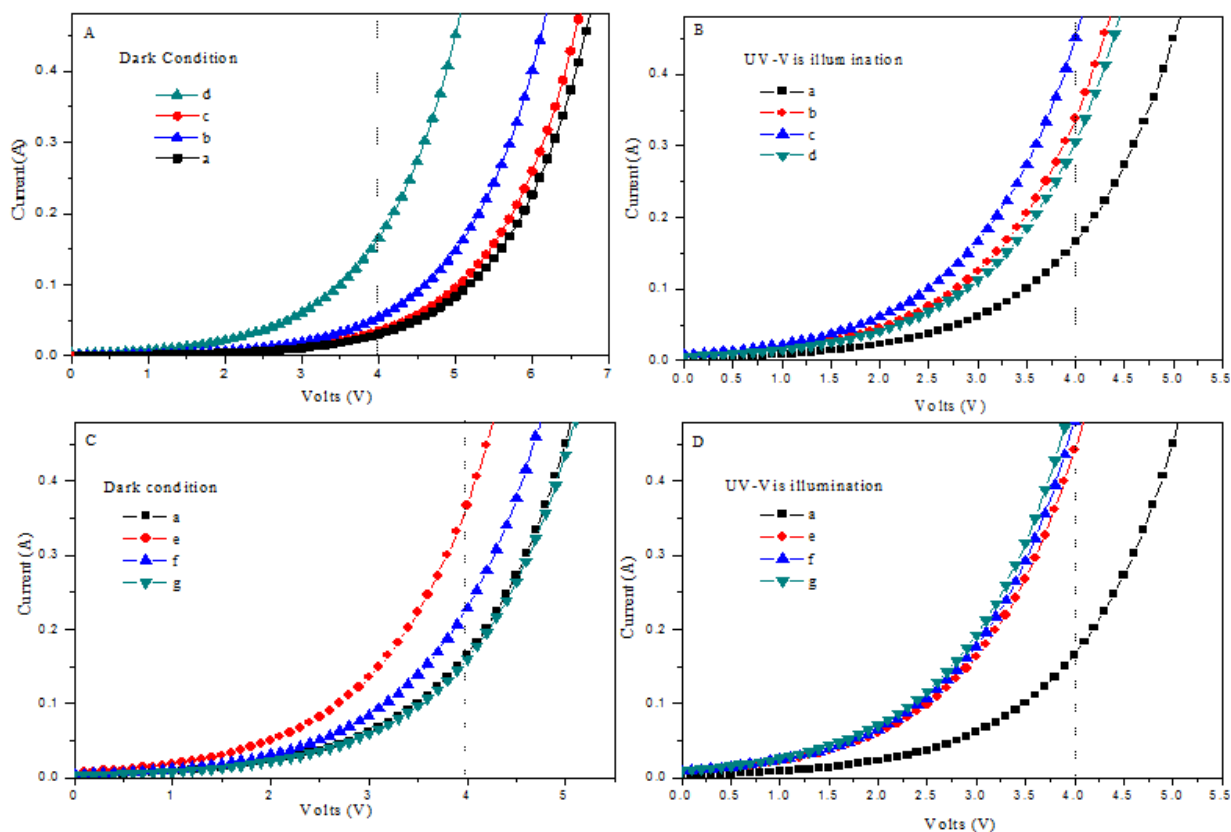


Figure 12. UV-Vis absorption spectra of Copper Phthalocyanine pigment adsorbed on ZnO and $\text{Cu}_{1-x}\text{Zn}_x\text{O}$ at different concentration. The films were soaked in a dye solution of 0.05 mM dye

Table 1. Content of the Lattice strain, Bond Length, Band gap calculated from XRD data and Conductance values measured in Dark and UV illumination, respectively

Sample	Lattice strain $\varepsilon [10^{-3}]$		Bond length [Å]	Band gap [eV]	Dark condition		UV-light illumination	
	a [1 0 0]	c [0 0 2]			Conductance [A]	Resistance [Ω]	Conductance [A]	Resistance [Ω]
a	4	3.6	5.3262	3.38	0.0292	34.247	0.1664	6.0096
b	3.6	2.7	5.3226	2.99	0.0354	28.249	0.3398	2.9429
c	3.6	3.9	5.3198	2.92	0.0546	18.315	0.4486	2.2292
d	3.3	3.6	5.3226	2.76	0.1654	6.0459	0.3062	3.2658
e	1	0.9	5.3253	2.17	0.367	2.7248	0.4421	2.2619
f	0.7	0.9	5.3304	2.16	0.2324	4.3029	0.4822	2.0738
g	1	0.9	5.3351	1.84	0.1624	6.1576	0.4914	0.2037

**Figure 13.** UV-Vis absorption spectra of Copper Phthalocyanine pigment adsorbed on ZnO and $\text{Cu}_{1-x}\text{Zn}_x\text{O}$ at different annealing temperature. The films were soaked in a dye solution of 0.05 mM dye**Figure 14.** Current-Voltage curves of ZnO and $\text{Cu}_{1-x}\text{Zn}_x\text{O}$ at different concentration (A) dark, (B) UV illumination. Current-Voltage curves of ZnO and $\text{Cu}_{1-x}\text{Zn}_x\text{O}$ at different annealing temperature (C) dark, (D) UV illumination

4. Conclusions

The optimization of semiconductors composition by the addition of any transition dopant is not the correct method to improve the efficiency of Cu-ZnO-DSSCs, the search for better dopant at optimized concentration and temperature could be considered as an alternative strategy. The results show that only in the ionic liquids, the Cu-ZnO hexagonal micro pyramids could be grown. The proposed microwave method is simple, easy to operate, less time consuming and inexpensive. It is observed that, dozens of smaller hexagonal pyramids are self-organized into a bigger ZnO pyramids. The results revealed, the peaks shift depends directly on the changes of the lattice, gradual enhancement of crystal growth along both *a* and *c*-axis and doping of Cu²⁺ ions. The Cu-ZnO powders annealed at higher temperature exhibits relatively lower absorption edge, which is shifted towards the longer wavelength region (IR range) compared to the samples annealed at lower temperature. The ratio between the forward and reverse current indicated that ZnO doped with Cu at higher concentration and at higher annealing temperature has a good rectification property. This method of preparation may be considered for efficient utilization of solar energy and industrialization.

Acknowledgments

Authors are grateful to the VGST (Vision Group on Science and Technology, Government of Karnataka, Bangalore) for the financial support (VGST-SMYSR/GRD-429). We are thankful to the Indian Institute of Science, Bangalore, for providing XRD, FESEM, EDAX analysis. The authors wish to thank the Department of Chemistry, Kuvempu University and the Rani Channamma University for providing laboratory facilities to carry out this work.

References

- [1] C.C. Vidyasagar, Y. Arthobanaik, T.G. Venkatesh, R. Viswanatha, Solid-state synthesis and effect of temperature on optical properties of Cu-ZnO, Cu-CdO and CuO nanoparticles. *Powder Tech.* 214 (2011) 337-343.
- [2] S. Rani, S. Poonam, P.K. Shishodia, R.M. Mehra, Synthesis of nanocrystalline ZnO powder via sol-gel route for dye-sensitized solar cells. *Solar Enrgy. Mater. Solar Cells.* 92 (2008) 1639-1645.
- [3] Y.Y. Ian Bu, Facile synthesis of highly oriented p-type aluminum co-doped zinc oxide film with aqua ammonia. *J. Alloys. Comp.* 509 (2011) 2874-2878.
- [4] U.G. Akpan, B.H. Hameed, The advancements in sol-gel method of doped-TiO₂ photocatalysts. *Appl. Catal., A.* 375 (2010) 1-11.
- [5] M. Law, L.E.; Greene, J.C. Johnson, R. Saykally, P. Yang, Nanowire dye-sensitized solar cells. *Nat. Mater.* 4 (2005) 455-459.
- [6] X.F. Gao, L. Jiang, *Nature.* 432 (2004) 36-38.
- [7] B. Panigrahy, M. Aslam, D. Bahadur, Effect of Fe Doping Concentration on Optical and Magnetic Properties of ZnO Nanorods. *Nanotechnol.* 23 (2012) 115601-115606.
- [8] J. Kaur, R.K. Kotnala, V. Gupta, K.C. Verma, Anionic Polymerization in Co and Fe Doped ZnO: Nanorods Magnetism and Photoactivity. *Current Appl. Phys. A.* 14 (2014) 749-756.
- [9] S. Kuriakose, B. Satpatib, S. Mohapatra, Enhanced Photocatalytic activity of co doped ZnO nanodisks and nanorods prepared by a facile wet chemical method. *Phy. Chem. Chem. Phys.* 16 (2014) 12741-12749.
- [10] L. Li, W. Wang, H. Liu, Liu, Q. Song, S. Ren, First Principles Calculations of Electronic Band Structure and Optical Properties of Cr-Doped ZnO. *J. Phy. Chem. C.* 113 (2009) 8460-8464.
- [11] M. Ahmad, E. Ahmed, Y.W. Zhang, N.R. Khalid, J.F. Xu, M. Ullah, Z.L. Hong, Preparation of Highly Efficient Al-Doped ZnO Photocatalyst by Combustion Synthesis. *Current Appl. Phys.* 13 (2013) 4697-704.
- [12] J.B. Zhong, Z. Li, X.Y. He, Zeng, Y. Lu, W. Hu, K. Lin, Improved Photocatalytic Performance of Pd-Doped ZnO. *Current Appl. Phys.* 12 (2012) 998-1001.
- [13] F.F. Ca, S. Xin, Y.G. Guo, L.J. Wan, *Phy. Wet Chemical Synthesis of Cu/TiO₂ Nanocomposites with Integrated Nano-Current Collectors as High Rate Anode Materials in Lithium-Ion Batteries. Phy.I Chem. Chem. Phys.* 13 (2011) 2014-2020.
- [14] M. Karimi, M. Ezzati, S. Akbari, Behtaj M. Lejbini, ZnO Microparticles, ZnO Nanoparticles and Zn_{0.9}Cu_{0.1}O Nanoparticles toward Ethanol Vapour Sensing: A Comparative Study. *Current Appl. Phys.* 13 (2013) 1758-1764.
- [15] B. Choudhary, S. Chawla, K. Jayanthi, K.N. Sood, S. Singh, Synthesis and Surface Modification of ZnO:Cu Nanoparticles by Silica and PMMA. *Current Appl. Phys.* 10 (2010) 3807-3812.
- [16] K.S. Ahn, S.Y. Yan, T. Shet, J. Deutsch, M. Al-Jassim, Enhanced photoelectrochemical response of ZnO films through Ga and N co-doping. *Appl. Phys. Lett.* 91 (2007) 231909-231912.
- [17] M. Gratzel, Recent advances in sensitized mesoscopic solar cells, *Acc. Chem. Res.* 42 (2009) 1788-1798.
- [18] M. Juddin, K. Iskandar, F. G. Okuyama, Stable photoluminescence of zinc oxide quantum dots in silica nanoparticles matrix prepared by the combined sol-gel and spray drying method. *J. Appl. Phys.* 89 (2001) 6431-6437.
- [19] P. Chand, A. Gaur, A. Kumar, Structural, optical and ferroelectric behavior of hydrothermally grown ZnO nanostructures. *Superlatt. Microstr.* 64 (2013) 331-342.
- [20] S. Kamarnen, M. Bruno, Synthesis of ZnO with and without microwaves. *Mater. Res. Bull.* 35 (2000) 1843-1847.
- [21] R.R. Bacsa, J. Dexpert-Ghys, M. Verelst, A. Falqui, B. Machado, W.S. Bacsa, P. Chen, S.M. Zakeeruddin, M. Graetzel, Synthesis and Structure-Property Correlation in Shape-Controlled ZnO Nanoparticles Prepared by Chemical Vapor Synthesis and their Application in Dye-Sensitized Solar Cells. *Adv.Funct. Mater.* 19 (2009) 875-886.
- [22] K.W. Gallis, C.C. Landry, Templated Gold Nanowire Self-Assembly on Carbon Substrates. *Adv. Mater.* 13 (2001) 1800-1803.
- [23] Z.W Pan, S.M. Mahurin, S. Dai, D.H. Lowndes, Lowndes, D. H. Nanowire Array Gratings with ZnO Combs. *Nano Lett.* 5 (2005) 723-727.
- [24] K.B. Suresh, L. Minoh, G.K. Man, J. Yong seok, J. Improvement of dye-sensitized solar cells toward the broader light harvesting of the solar spectrum, *Chem. Commun.* 49 (2013) 1471-1487.
- [25] C. Prakash, G. Anurag, K. Ashavani, Effect of Cr and Fe Doping on the Structural and Optical Properties of ZnO Nanostructures. *Inter. J. Chem. Molecular, Nuclear Mater. Metallug. Eng.* 8 (2014) 12-17.
- [26] X. X. Zhou, J. Zhao Zhi Yuan, K. Qin, Z. Shu-Hong, X. Tao, H. Rong-Bin, Z. Lan-Sun, Formation of ZnO hexagonal micro-pyramids; a successful control of the exposed polar surfaces with assistance of an ionic liquid. *Chem. Commun.* 2 (2005) 5572-5574.
- [27] S. Mohammad, B. Sunayna, M.M. Muhammad, L. Jianlin, Realization of Cu-Doped p-type ZnO thin films by molecular beam epitaxy. *ACS Appl. Mater. Interfaces.* 7 (2015) 8894-8899.
- [28] H.M. Galindo, Y. Carvajal, E. Njagi, R.A. Ristau, S.L. Suib, Facile one-step template-free synthesis of uniform hollow microstructures of crypto melane-type manganese oxide K-OMS-2. *Langmuir.* 26 (2010) 13677-13683.
- [29] C. Dewei, L. Sean, Growth and Electrical Properties of Doped ZnO by Electrochemical Deposition. *New J. Glass Ceram.* 02 (2012) 13-16.
- [30] C. C. Vidyasagar, Mohammed Khenfouch, Prakash Kariyajjanavar, Green Microwave Combustion Synthesis Cr-ZnO Nanocrystals and Effect of Cr²⁺ on Structural and Electrical Properties, *Adv. Sci. Eng. Med.* 9 (2017) 810-815.
- [31] C.C. Vidyasagar, Y. Arthoba Naik, Surfactant (PEG 400) effects on crystallinity of ZnO nanoparticles, *Arabian J. Chem.* (2016) 9, 507-510.
- [32] B.E. Hardin, E.T. Hoke, P.B. Armstrong, Y. Jun-Ho, P. Comte, T. Torres, J.M.J. Frechet, K. Nazeeruddin, M. Gratzel, M.D.

McGehee, Increased light harvesting in dye-sensitized solar cells with energy relay dyes. *Nat. Photonics*. 3 (2009) 406-411.

- [33] R.O. Yathisha, Y. Arthoba Nayaka, C.C. Vidyasagar, Microwave combustion synthesis of hexagonal prism shaped ZnO nanoparticles and effect of Cr on structural, optical and electrical properties of ZnO nanoparticles, *Mater. Chem. Phys.* 181 (2016) 167-175.
- [34] A.K. Singh, Synthesis, characterization, electrical and sensing properties of ZnO nanoparticles. *Adv. Powder Tech.* 21 (2010) 609-613.



© The Author(s) 2019. This article is an open access article distributed under the terms and conditions of the Creative Commons Attribution (CC BY) license (<http://creativecommons.org/licenses/by/4.0/>).